*J. Electrochem. Sci. Eng.* **14(4)** (2024) 487-498; http://dx.doi.org/10.5599/jese.2140

Open Access : : ISSN 1847-9286
www.jESE-online.org

*Original scientific paper*

# The solid particle erosion performance of tungsten inert gas yttria-stabilized zirconia - Inconel 625 composite cladding

Neeraj Kamboj[1,✉], Lalit Thakur[1] and Manpreet Kaur Arora[2]

[1]*Mechanical Engineering Department, National Institute of Technology,Kurukshetra, Haryana, 136119, India*

[2]*Mechanical Engineering Department, Baba Banda Singh Bahadur Engineering College, Fatehgarh Sahib, Punjab,140407, India*

*Corresponding authors:* ✉*neeraj_6180090@nitkkr.ac.in*

Received: October 20, 2023; Accepted: February 4, 2024; Published: March 4, 2024

***Abstract***

*The yttria-stabilized zirconia (YSZ) - Inconel 625 (IN625) composite cladding was deposited on a stainless steel substrate using a tungsten inert gas welding manipulator to protect it from solid particle erosion. Erosion wear tests were carried out at room temperature according to the ASTM G76-18 procedure. The surface of the tested material was exposed to a jet of alumina erodent particles at impact angles of 30 and 90°, respectively. Scanning electron microscopy images were utilized to examine the morphologies of the eroded surface and the microstructure of cladding. The erosive performance of YSZ - IN625 composite cladding was 3.5 and 2.4 times compared to the substrate at different impact angles. Improved microhardness and fracture toughness resulting from the favourable interaction between the hard ceramic YSZ particles and the IN625 matrix led to the enhanced erosion performance of composite cladding. Micro-cutting and ploughing were the predominant wear mechanisms in the substrate during the solid particle erosion test at a 30° impact angle, whereas the indentation-induced plastic deformation was dominant at a 90° impact angle. The results also revealed that the micro-cutting, detached splats and fissures were responsible for the wear in composite cladding at 30 and 90° impact angles.*

**Keywords**

Air jet erosion; hardness; fracture toughness; wear

## Introduction

The deterioration of materials is a crucial concern for all manufacturing industries. Materials degradation often causes complete system failure. Abrasion, adhesion, corrosion, erosion, and surface fatigue are the most frequent types of wear that cause components to degrade. Abrasive, adhesive, and erosion wear are the primary types that significantly affect the financial losses and

maintenance costs of the various components. Erosion induced by impinging hard microscopic particles poses a significant challenge in petrochemical, turbine blades and food processing industries [1]. These industries' mechanical components must be protected on their working surfaces to prevent early failure [2,3]. Consequently, wear-resistant alloys or coatings are advised to counteract the erosion problems. The use of protective coating is a cost-effective approach to protect the components because the alloys with excellent wear and corrosive properties are very costly and always find difficulty in processing into some working component [4].

The tungsten inert gas (TIG) weld cladding process has become more popular in creating wear-resistant coatings compared to other surface modification techniques such as laser, electron beam and thermal spraying [5-8]. The high temperature and constrained cladding thickness are significant issues with thermal spray coatings. The TIG weld cladding method aims to achieve the desired mechanical and tribological capabilities by changing the composition and microstructure of the substrate surface without compromising the bulk properties [9,10]. Ni-based alloy claddings developed using the TIG weld cladding technique have demonstrated exceptional performance against wear at room and elevated temperatures [11-13]. It is well known that Ni-based alloys have several advantages, including high hardness, enhanced wear and erosion resistance. Additionally, alloys composed of nickel with high chromium concentrations are frequently used as corrosion-resistant coating materials owing to their remarkable resistance to oxidation and corrosion [14-16]. The TIG weld cladding can effectively protect the underlying substrate by producing a protective chromium oxide layer at high temperatures. These $Cr_2O_3$ protective oxide layers are stable, which creates a thick, continuous, and adherent layer that prevents the oxygen from contacting the coating or underlying substrate [7,17].

One study examined the erosion behaviour of 73Ni-13Cr-4Sn-4Bi-Mo alloy. The results showed that the material's erosive resistance is strongly correlated with the impact energy and velocities of the erodent [18]. Another research looked at how impact angle and testing duration affected the erosion of stainless steel (s.s.) at higher velocities. It found that the maximum depth of cut increased as the testing duration increased and peaked at an impact angle of 40°. At low-impact angles, the indentation-induced plastic deformation mechanism was dominant, but at high-impact angles, the micro-cutting/ploughing mechanism was predominant [19,20]. In an additional investigation, the behaviour of solid particle erosion in tungsten carbide (WC)-reinforced Ni-matrix-based laser-clad layers was examined to enhance the engineering components' performance for possible power plant applications. The findings showed that impact angle and erodent jet velocity are the main factors controlling the eroding behaviour of the WC-Ni laser clad. Signature wear at the erosion wear surface showed that ductile erosion processes controlled the erosion mainly, with WC particles being removed from the matrix as a secondary factor [21]. According to different research, micro-cutting and micro-fissuring were the main processes for the generation of mass losses during solid particle erosion in the erosive wear of Inconel 625 alloy coatings applied using the cold metal transfer (CMT) technique [22].

The inclusion of different ceramics like TiC, SiC, WC, $Al_2O_3$, etc., has established new upper limits for corrosion, oxidation, erosion, and wear resistance of Ni-based alloys [23-26]. The yttria-stabilized zirconia (YSZ) ceramic material is increasingly used for room and high-temperature environments where it exhibits high corrosion and wear resistance because it generates a solidly adherent $ZrO_2$ surface film [23,27-29]. The prevention of ferrous alloys (carbon and stainless steel) components in various industries from solid erosion is an important area of research. In this research, 304 stainless steel substrates were cladded with Inconel 625 + YSZ (25 wt.%) powder using the TIG weld cladding

process. Claddings' microhardness and fracture toughness have been calculated and compared with the substrate. The erosion behaviour of claddings was assessed using an air jet erosion test machine. The wear mechanism in worn-out claddings was examined using scanning electron microscopy (SEM) images.

## Experimental

### *Materials and tungsten inert gas cladding*

The AISI 304 stainless steel with dimensions of 25×25×5 mm was used as the substrate material. In this investigation, Inconel 625 (G.S.P., Mumbai, India) and YSZ (Mincometal, Bengaluru, India) powders with particle sizes of 15-50 and 30-50 µm, respectively, were considered for cladding deposition. The powder Inconel 625 (IN625) SEM images at 500× and 1,000× magnifications are displayed in Figure 1(a-b). The IN625 particles, which range in size from 15 to 50 µm, have a spherical shape. The IN625 powder's energy dispersive spectroscopy (EDS) spectrum is seen in Figure 1c.

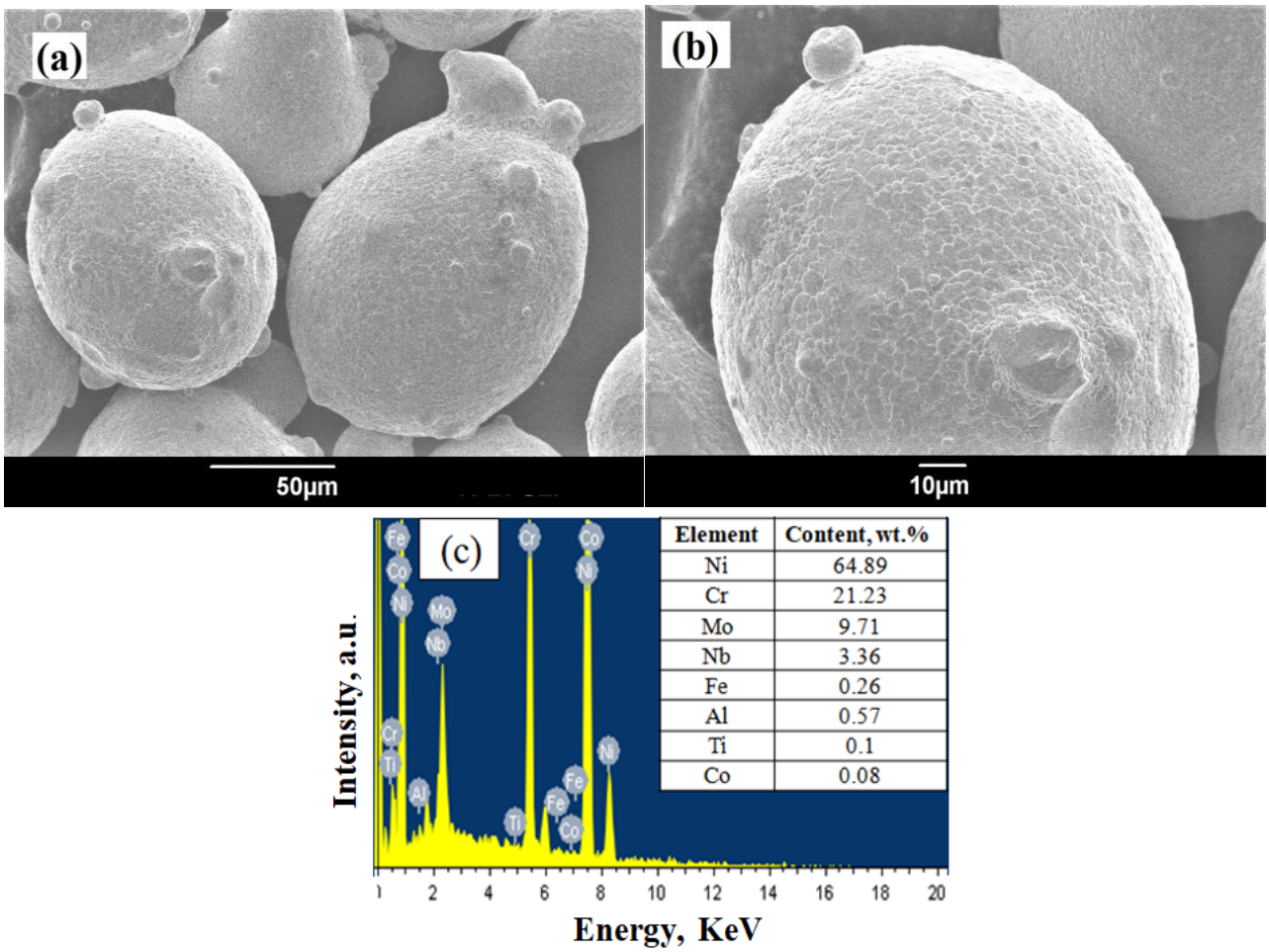


***Figure 1.*** *SEM image of IN625 powder at (a) 500X (b) 1,000X, and (c) EDS spectrum of IN625 powder*

The primary elements found in the IN625 powder, according to EDS, are Ni, Cr, Mo, and Nb. Mechanical mixing of the Inconel 625 and YSZ (25 wt.%) powders was performed in a jar milling machine for 2 h. With this powder and polyvinyl alcohol (PVA. in 10 wt.%) [9] binder, a semisolid paste was created. The Inconel 625-YSZ (25 wt.%) + PVAbinder paste was applied evenly to the specimen's top surface. A 3-axis CNC-controlled TIG welding equipment was used to deposit the Inconel 625-YSZ (25 wt.%) claddings. The optimized process parameters were taken from the authors' previous study and optimized for room temperature wear performance, as indicated in Table 1 [18]. Figure 2 depicts

the process diagram of the TIG weld cladding technique. Figure 3(a-c) displays an SEM image, EDS spectra and XRD of powders containing a mixture of IN625 and YSZ (25 wt. %), respectively.

***Table 1**. TIG weld cladding process parameters used in the present work [23]*

| Parameters | Current, A | Welding speed, mm min$^{-1}$ | Standoff distance, mm | YSZ concentration, wt.% |
|---|---|---|---|---|
| Value | 70 | 192 | 2 | 25 |

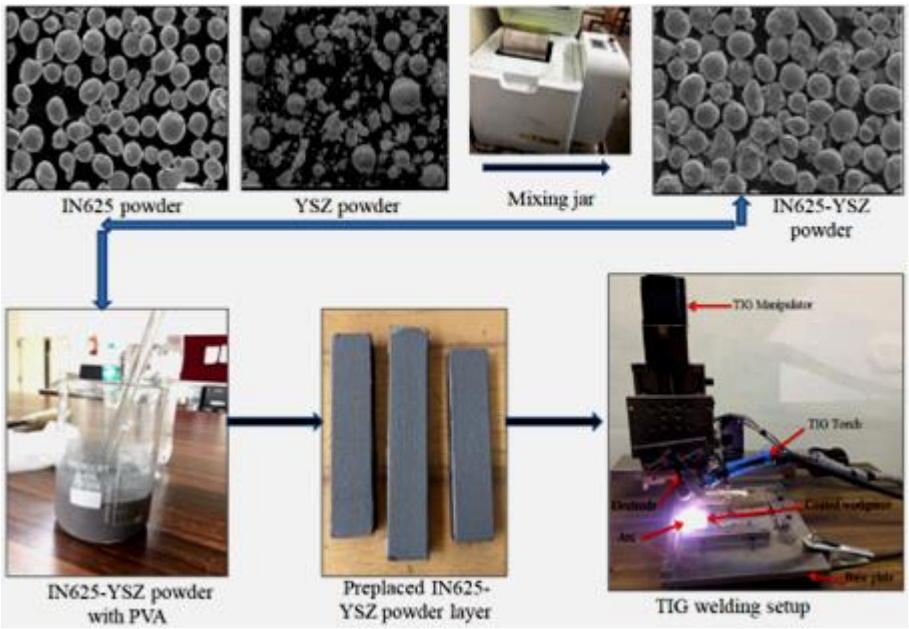


***Figure 2.** Process diagram for the TIG weld cladding*

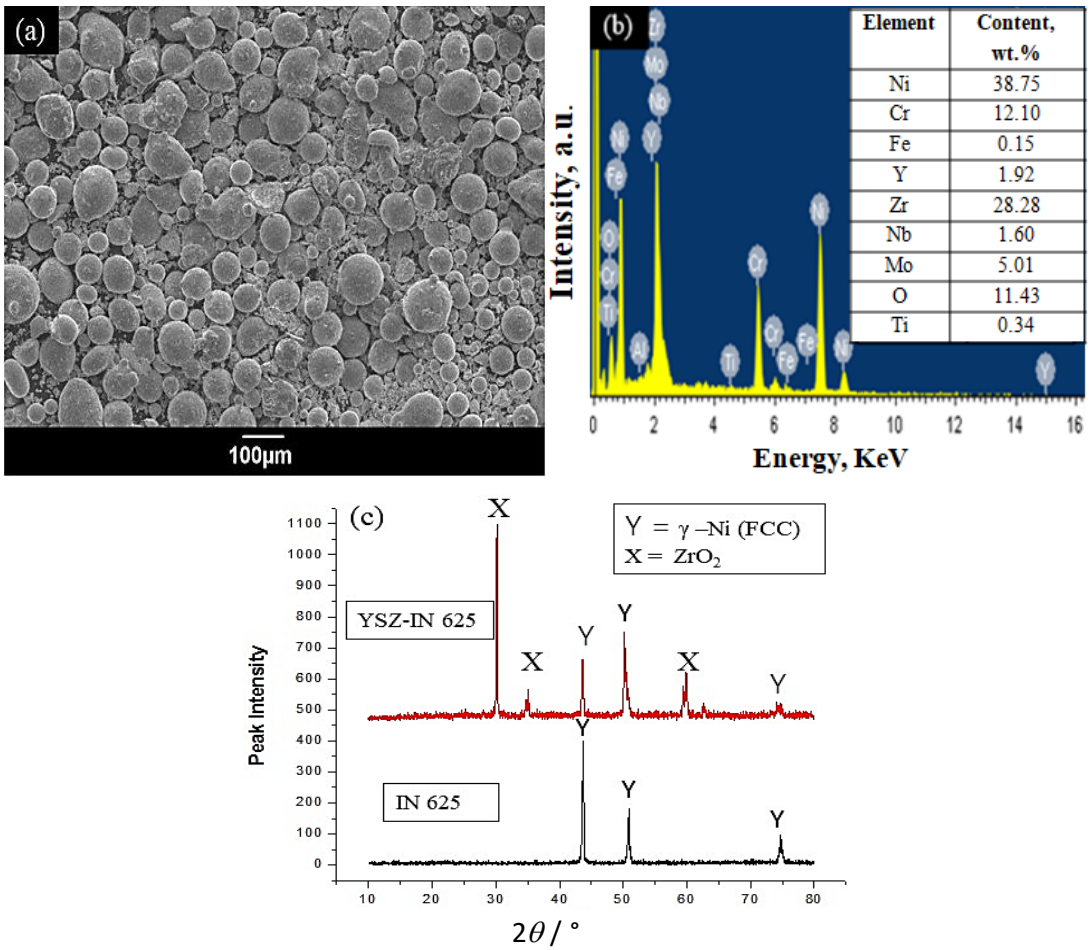


***Figure 3.** (a) SEM image, (b) EDS spectra and (c) XRD of IN625 and YSZ-IN625 powders*

*Characterization techniques*

A scanning electron microscope (JEOL JSM-6390LV) (SEM) with an energy dispersive spectroscopy (EDS) attachment and optical microscopy (OM) were used to perform the microstructural characterization of the claddings. To achieve a mirror-like polished cross-section and a smooth surface, the cut specimens were polished using emery grades ranging from 200 to 2,000 grit numbers using a double disc-polishing machine (Banbros Engineering Pvt. Ltd., India). An etchant was used to investigate the grain structure of claddings. Etchant was prepared by adding 15 mL HCl, 10 mL acetic acid, and 10 mL $HNO_3$ and then gently used on a polished surface for 20-30 s. A diffractometer (D8 Advance, Bruker, Germany) with CuKα radiation was used for the XRD analysis to identify the developed phase in the claddings. The cladding's microhardness was measured over the polished cross-section with the help of a Vicker's microhardness tester (XHVT-1000Z, China) at a 300 g load and 15 s dwell time. The mean microhardness value was determined by taking ten indents and reported in the current study. To evaluate the cladding's fracture toughness, ten indents were generated by a Vickers hardness tester through a substantial load of 10 kg. The cladding's fracture toughness was calculated using the Equation (1) [30]:

$$K_{IC} = 0.079\left(\frac{p}{b}\right)^{\frac{3}{2}} \log\left(4.5\frac{b}{z}\right) \quad (1)$$

Here $p$ / kg is load, $b$ / µm is half diagonal length, $z$ / µm is the crack length from the indented centre.

*Erosion test*

An air erosion test according to ASTM G76-18 was carried out at ambient temperature using an air jet erosion test rig (TR-471-600, DUCOM-Bangalore, India) to investigate the erosion behaviour of the cladding. The working principle and position of the cladding workpiece are illustrated in Figure 4. The testing was performed using the alumina ($Al_2O_3$) erodent with particle sizes of around 50 µm. Figure 5 displays the SEM image of the alumna erodent used in this research. As per ASTM G7-18 standard, the powder feeding rate was set to 2 g $s^{-1}$, and the nozzle was placed 10 mm away from the workpiece. To evaluate the erosion behaviour of all samples, tests were conducted at two different angles, 30 and 90° [24,30], respectively. Furthermore, the erodent exposure time was set to 10 minutes.

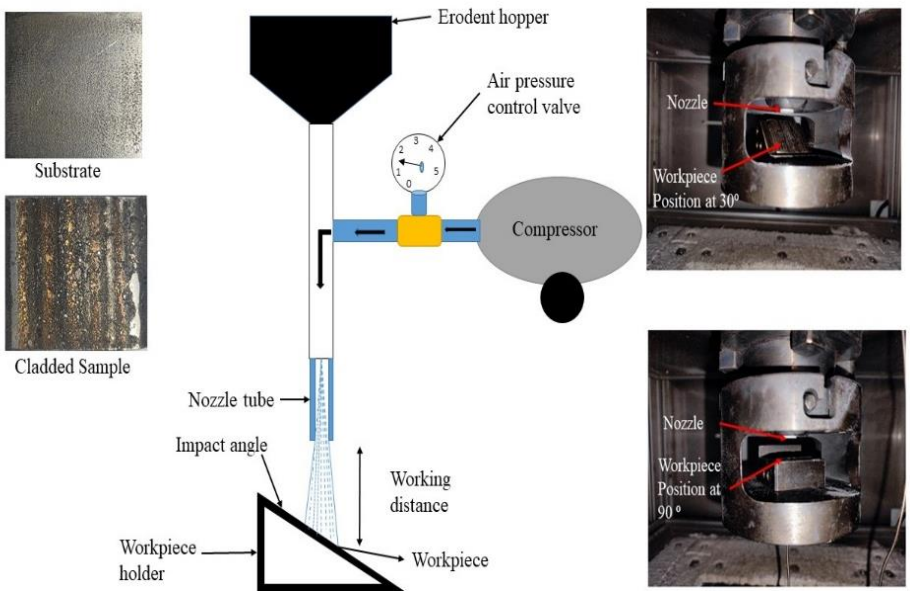


***Figure 4**. Systematic view of air jet erosion testsetup with workpiece positions*

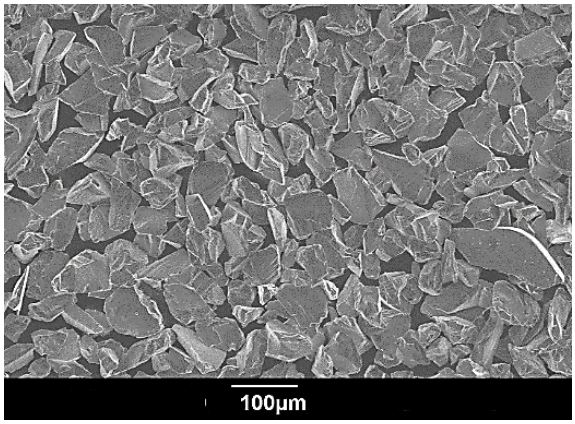


***Figure 5**. SEM image of alumina erodent*

## Results and discussion

*As-deposited composite cladding characterization*

The surface morphology of as-deposited cladding is shown in Figure 6a. The YSZ particles appeared to be immersed in the matrix of IN625. The scattered YSZ particles (mostly partially melted) are consistently dispersed throughout the as-deposited cladding microstructure. Figure 6b-6c shows a cross-sectional SEM image and XRD pattern of the deposited cladding. The SEM image shows appropriate metallurgical bonding between composite cladding and the stainless steel substrate. Moreover, there are no cracks, and a smaller heat-affected zone has been developed in the cladding. XRD image shows a peak of γ- Ni-Cr-Fe along with $Cr_2O_3$ and $ZrO_2$ stable oxides phases. Inconel 625 powder primarily comprises Ni, Cr, and Fe elements. Figure 6d shows that cladding exhibited a dense microstructure with significant dendrites and an equiaxed type of grain growth.

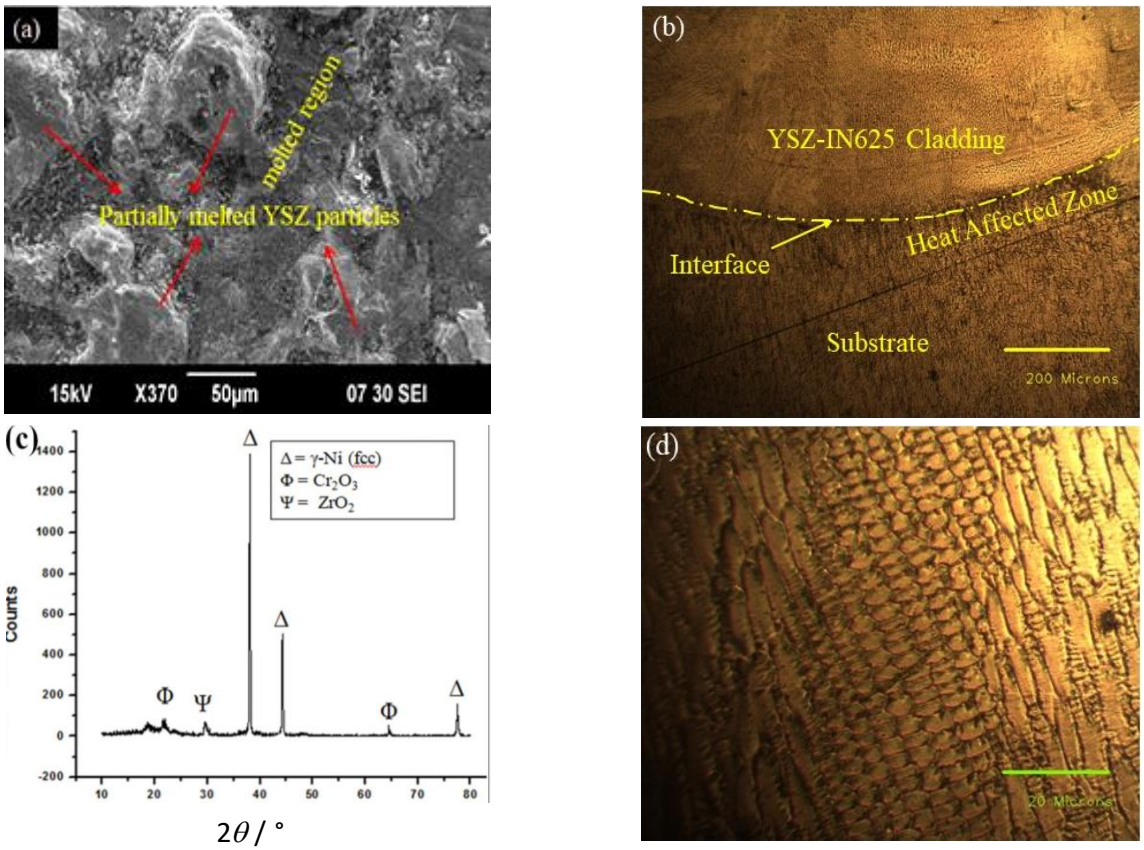


***Figure 6**. (a) SEM image of deposited cladding, (b) Cross-sectional SEM image of cladding along with substrate at lower magnification, (c) XRD, (d) SEM image of cladding at higher magnification*

Figure 7 (a-b) displays the EDS analysis of uncladded (substrate) and cladding samples. As revealed from EDS analysis, the substrate's primary constituents are Fe, Cr, and Ni. In contrast, a rich composition of elements like Ni, Cr, Zr, Mo, Nb and Fe has been observed in the cladding. The increase of Fe in the cladded sample could be explained by the dilution of the substrate matrix, which is essential for good metallurgical bonding with the substrate.

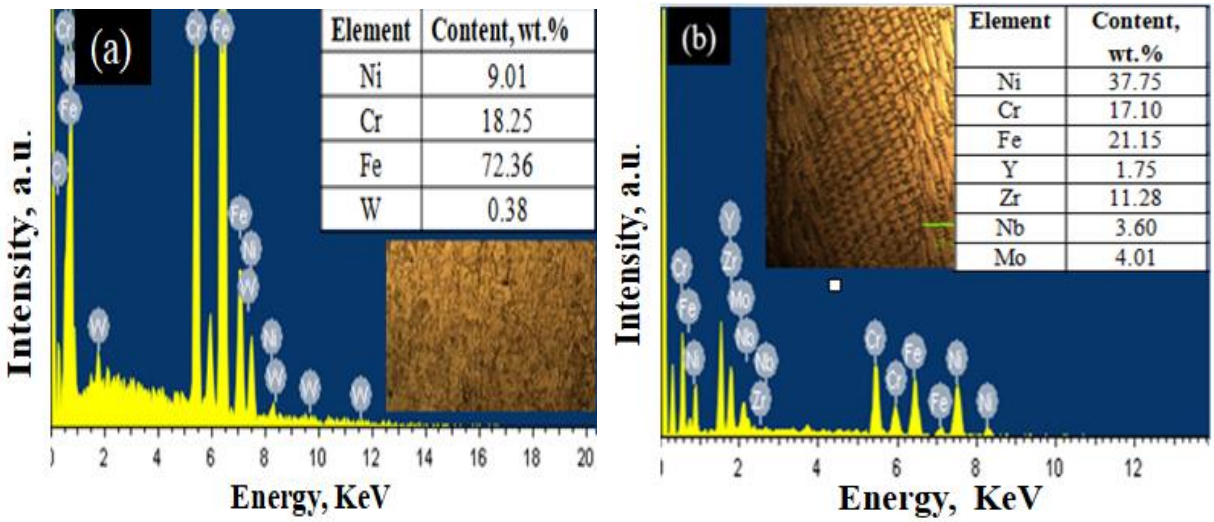


***Figure 7.*** *(a-b) EDS result of uncladded sample (AISI 304 SS substrate) and cladded sample, respectively*

*Microhardness and fracture toughness analysis*

The microhardness of the substrate and cladding was measured by a Vickers microhardness tester at 300 g load and 15 s dwell time. The average microhardness for the substrate (stainless steel 304) and cladding was found to be 140 ± 5 $HV_{0.3}$ and 330 ± 4 $HV_{0.3}$, respectively, as shown in Figure 8a. The strain-hardening effect induced by strengthening elements such as Ni, molybdenum, and niobium existing in the cladding is responsible for this increase in microhardness [11,23]. This increase in hardness is also due to the difference in the coefficients of thermal expansion of YSZ and Inconel 625. This variation causes geometric dislocations (GD) and the pinning of dislocation motions at their edges by hard particles, resulting in matrix strain hardening [14]. The microhardness variation across the cross-sectional area and heat-affected zone (HAZ) are presented in Figure 8a.

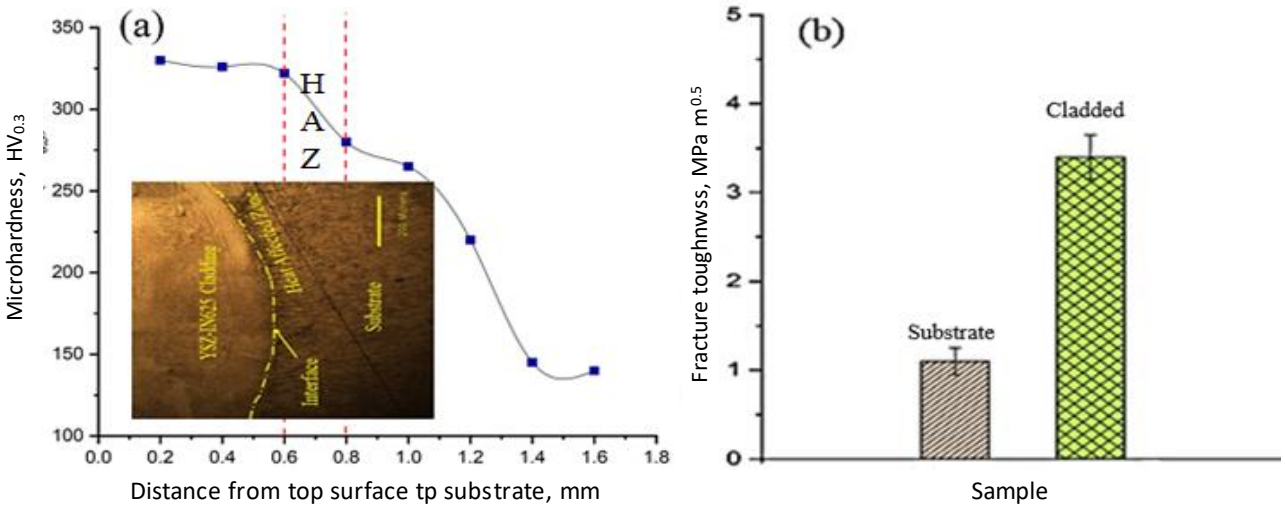


***Figure 8.*** *(a) Vicker's microhardness distribution (b) fracture toughness values*

The heat-affected zone (HAZ) is that area of metal that has not been melted and has undergone changes in properties due to exposure to relatively high temperatures during TIG welding. The fracture toughness of substrate and cladding was found to be 1.1±0.04 and 3.4±0.06 MPa $m^{1/2}$, respectively. The high fracture toughness value of the cladding can be related to strain hardening and pinning effects caused by hard particles. The YSZ hard particles in composite cladding enhance fracture energy due to crack front blunting [31,32]. Figure 8b shows the fracture toughness values of substrate and cladding.

*Effect of impingement angle on erosion (air-jet erosion test)*

The solid particle erosion test was performed at 30 and 90° angles on the uncladded substrate and the cladding specimens. Figure 9a - 9d summarises optical pictures of the degraded surfaces of the substrate and cladded workpieces exposed to different test angles. It was discovered that cladded samples experienced less damage compared to the substrate at all the impingement angles. Figures 9a and 9b indicate that both testing angles leave a deeper impression on the substrate. In contrast, the surface of claddings has the most minor imprints (Figure 9c - 9d). Figure 9e depicts substrate and claddings' erosive wear (weight loss). In the cladded sample, the erosion rate is governed by the composition of cladding material [24,30]. The outcomes show that the erosive wear resistance of cladding samples is almost 3.5 times and 2.4 times better than uncladded samplesat 30 and 90° impingement angles, respectively. The composite cladding's superior performance can be attributed to its high hardness and fracture toughnes. As already stated, the YSZ-IN625 claddings have a high fracture toughness, which leads to higher erosion resistance. The YSZ particle reinforcement in the claddings helps to strengthen the IN625 matrix by dispersion. As a result, the reinforced claddings' microhardness and erosive resistance have increased even further. Furthermore, stable oxides such as $Cr_2O_3$ and $ZrO_2$ helped to improve composite claddings' erosion resistance.

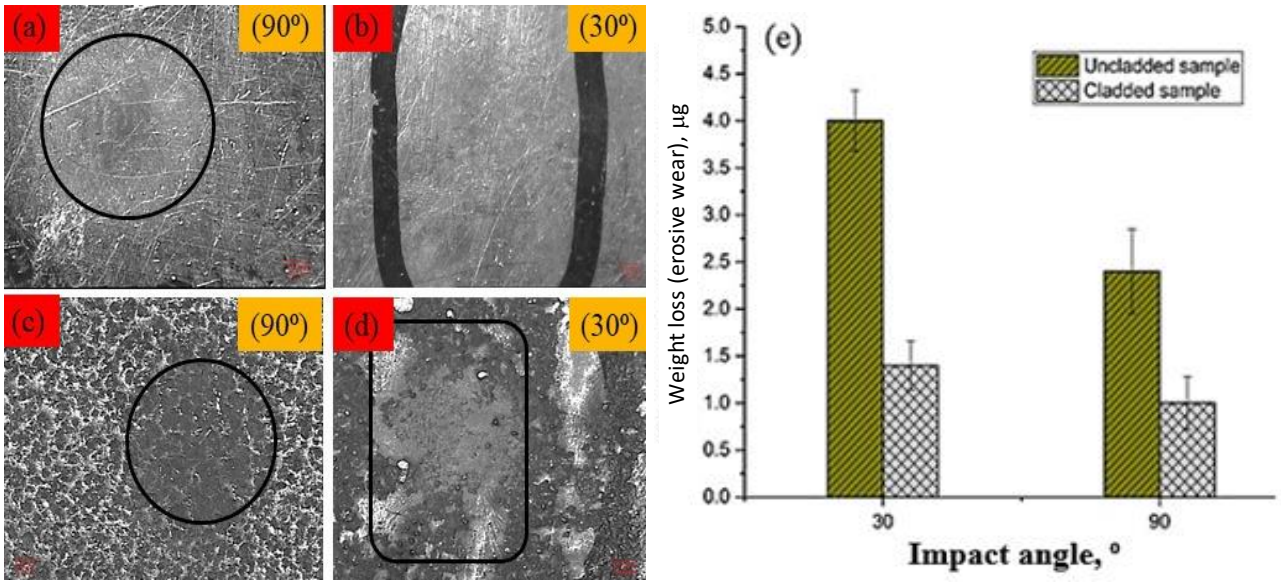


***Figure 9.*** *(a-d) Optical pictures of the degraded surfaces of both (substrate and cladding) (e) weight loss Impact angle of the substrate and cladded sample at different impact angles*

*Erosion mechanism*

SEM images were used to investigate the erosive mechanism of the damaged outer layer of the substrate and cladding samples. Figure 10 (a-d) shows the surface morphology of the substrate and cladded samples subjected to the erosion test. At a 30° impact angle, material removal occurs in uncladded samples due to the micro-cutting and ploughing caused by the sharp edges of the

erodent, as shown in Figure 10a. Apart from that, some minor craters and cavities were also generated. Figure 10b shows the formation of craters due to the repetitive collision of eroded particles resulting in the pull-out of debris at a 90° impact angle. Material detachment from the groove indicates erosive wear. As a result, it is possible to conclude that the substrate exhibits a ductile erosion mechanism, in which the material predominantly fails via plastic deformation [30]. Indentation-induced plastic deformation was dominant at a 90° impact angle [20]. Maximum material removal happens at 30°, while less removal occurs at 90°.

As demonstrated in Figure 10c, micro-cutting and ploughing are significant erosion mechanisms that contribute to removing the material from the cladded sample. The SEM picture of degraded cladding revealed numerous abrasion markings with little plastic distortion and a few small grooves developed on the outer layer at a 30° impact angle, as illustrated in Figure 10c. At a 30° angle, the erodent imposes a powerful repeated tangential force onto the intended surface. This tangential force removed certain unmelted particles of the cladding, leaving behind traces of minor craters. The uniformly dispersed YSZ particles bind the IN625 matrix and limit the plastic deformation of the cladding in contrast to the uncladded sample. At a 90° impact angle, the impact of erosive particles on the splats led to the accumulation of debris liberated from the IN625 matrix at the location of impingement and the removal of a significant amount of material from the outer layer. The crater was formed by removing a chunk of material from the surface. Furthermore, as illustrated in Figure 9d, the impact created by the erodent is passed to the unmelted YSZ particles, producing cracks and contributing to crack propagation. A schematic representation of different types of plastic deformation by solid particles is presented in Figure 11.

YSZ-IN625 claddings exhibit superior erosion resistance to uncladded samples at all impact angles. The YSZ-IN625 composite cladding has higher fracture toughness and hardness values. An optimum mix of the microhardness and fracture toughness resulted from the favourable interaction between the hard ceramic YSZ particles with the IN625 matrix, which helped to enhance the erosion performance of YSZ-IN625 composite cladding.

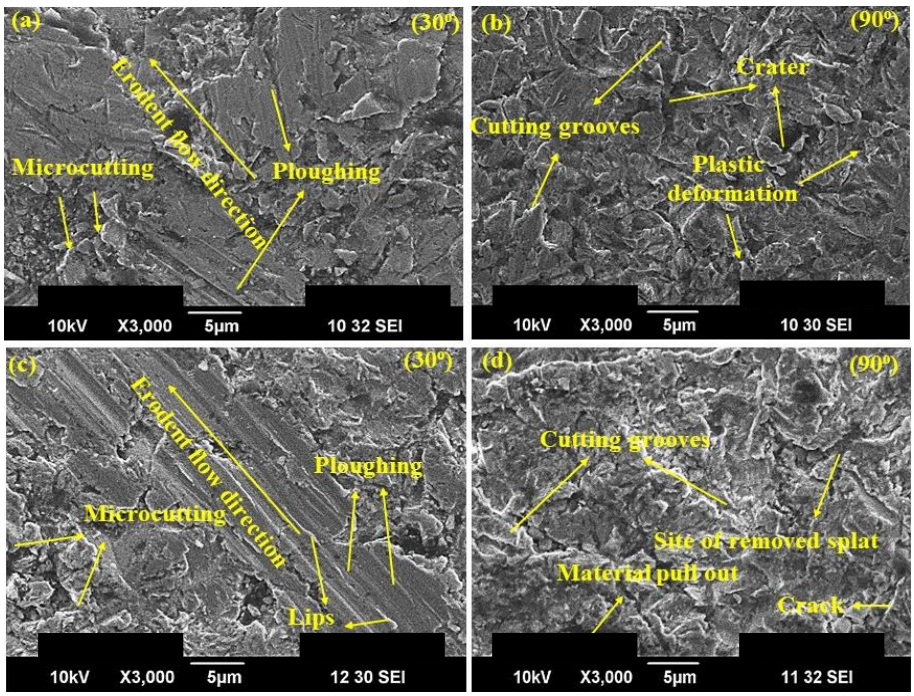


***Figure 10**. SEM images of (a-b) substrate and (c-d) YSZ-IN625 cladding eroded areas with impingement angles*

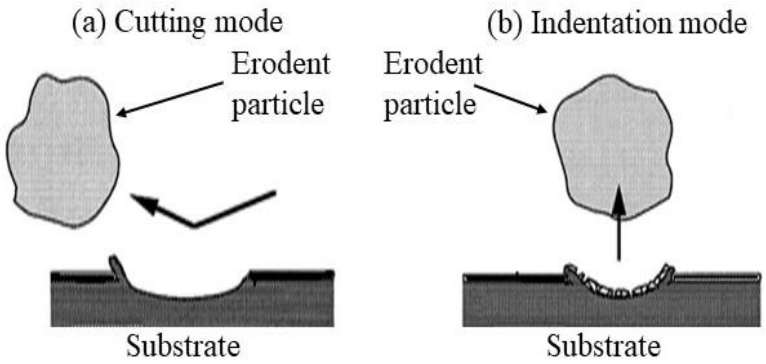


***Figure 11.*** *Schematic representation of different types of plastic deformation by erodent (a) cutting mode at 30° and (b) indentation mode at 90°*

## Conclusion

A YSZ-Inconel 625 composite cladding was developed using the TIG weld cladding technique and was analysed for its erosion performance. The following are the prominent conclusions of the current research:

- The cross-section of the produced cladding demonstrated a good metallurgical bonding with the substrate without any sign of cracking and high dilution.
- The microhardness value of the cladding was 330 $HV_{0.3}$, which is 2.5 times better than that of the substrate (140 $HV_{0.3}$).
- The fracture toughness test revealed that the cladding had a maximum toughness value of 3.4 MPa $m^{0.5}$ compared to the substrate's toughness value of 1.1 MPa $m^{0.5}$.
- The various stable phases and oxides, like γ- Ni, $Cr_2O_3$, and $ZrO_2$, acted as a protective layer and contributed to better erosion resistance.
- The partially melted YSZ particles retained their original shape in the cladding, resulting in a compact dendrite (IN625) and an equiaxed (YSZ) structure of grains, significantly enhancing the microhardness and resistance to erosion.
- The grooves and craters on surfaces indicate that the erosion mechanism comprises ploughing, micro-cutting, and indentation-induced plastic deformation for the substrate. The mechanisms of degradation in claddings at 30 and 90° impact angles included micro-cutting, detached splats, and cracks. The erosive wear performance of YSZ-IN625 cladding enhanced approximately 3.5 times at 30° and 2.4 times at 90° impact angles.

***Acknowledgements****: This research received no specific grant from any funding agency in the public, commercial, or not-for-profit sectors.*

***Conflicts of interest****: The authors also declare that they have no conflict of interest.*

## References

[1] Z. Azakli, R. Gümrük, Particle Erosion Performance of Additive Manufactured 316L Stainless Steel Materials, *Tribology Letters* **69** (2021) 130. https://doi.org/10.1007/s11249-021-01503-0

[2] N. Kaur, M. Kumar, S .K. Sharma, D. Young, S. Kumar, N. M. Chavan, S. V Joshi, N. Singh, H. Singh, Applied Surface Science Study of mechanical properties and high temperature oxidation behavior of a novel cold-spray Ni-20Cr coating on boiler steels, *Applied Surface Science* **328** (2015) 13-25. https://doi.org/10.1016/j.apsusc.2014.12.033

[3] M. Naveed, H. Schlag, F. König, S. Weiß, Influence of the Erodent Shape on the Erosion Behavior of Ductile and Brittle Materials, *Tribology Letters* **65(18)** (2017) . https://doi.org/10.1007/s11249-016-0800-x
[4] J. H. Tylczak, Erosion-corrosion of iron and nickel alloys at elevated temperature in a combustion gas environment, *Wear* **302** (2013) 1633-1641. https://doi.org/10.1016/j.wear.2013.01.008
[5] J. Singh, L. Thakur, S. Angra, Abrasive wear behavior of WC-10Co-4Cr cladding deposited by TIG welding process, *International Journal of Refractory Metals and Hard Materials* **88** (2020) 105198. https://doi.org/10.1016/j.ijrmhm.2020.105198
[6] S. Saroj, C.K. Sahoo, M. Masanta, Microstructure and mechanical performance of TiC-Inconel825 composite coating deposited on AISI 304 steel by TIG cladding process, *Journal of Materials Processing Technology* **249** (2017) 490-501. https://doi.org/10.1016/j.jmatprotec.2017.06.042
[7] N. Kamboj, L. Thakur, A study of processing and high-temperature sliding wear behaviour of Inconel-625 alloy TIG weld cladding, *International Journal of Materials Engineering Innovation* **13** (2022) 1. https://doi.org/10.1504/ijmatei.2022.10045603
[8] N. Kamboj, L. Thakur, Tribology International Experimental investigation of the high temperature sliding wear behaviour of RSM optimized YSZ-Inconel 625 TIG weld cladding, *Tribology International* **187** (2023) 108741. https://doi.org/10.1016/j.triboint.2023.108741
[9] J. Singh, L. Thakur, S. Angra, Effect of argon flow rate and standoff distance on the microstructure and wear behaviour of WC-CoCr TIG cladding, *Journal of Physics: Conference Series* **1240** (2019). https://doi.org/10.1088/1742-6596/1240/1/012162
[10] [J. Singh, L. Thakur, S. Angra, A study of tribological behaviour and optimization of WC-10Co-4Cr Cladding, *Surface Engineering* **37** (2021) 70-79. https://doi.org/10.1080/02670844.2020.1745367
[11] S. S. Sandhu, A. S. Shahi, Metallurgical, wear and fatigue performance of Inconel 625 weld claddings, *Journal of Materials Processing Technology* **233** (2016) . https://doi.org/10.1016/j.jmatprotec.2016.02.010
[12] R. Ranjan, A. Kumar Das, Protection from corrosion and wear by different weld cladding techniques, *Materials Today: Proceedings* **57** (2022) 1687-1693. https://doi.org/10.1016/j.matpr.2021.12.329
[13] R. Panwar, P. Chandna, Parameter optimization of FSW aviation-grade AA8090 using Taguchi grey relational analysis, *Aircraft Engineering and Aerospace Technology* **95** (2023) 715-724. https://doi.org/10.1108/AEAT-05-2022-0118
[14] G. Sreedhar, M. M. Alam, V. S. Raja, Hot corrosion behaviour of plasma sprayed YSZ/$Al_2O_3$ dispersed NiCrAlY coatings on Inconel-718 superalloy, *Surface and Coatings Technology***2 04** (2009) 291-299. https://doi.org/10.1016/j.surfcoat.2009.07.026
[15] A. Bakkar, M. M. Z. Ahmed, N. A. Alsaleh, M. M. E. S. Seleman, S. Ataya, Microstructure, wear, and corrosion characterization of high TiC content Inconel 625 matrix composites, *Journal of Materials Research and Technology* **8** (2019) 1102-1110. https://doi.org/10.1016/j.jmrt.2018.09.001
[16] H. Y. Al-Fadhli, J. Stokes, M. S. J. Hashmi, B. S. Yilbas, The erosion-corrosion behaviour of high velocity oxy-fuel (HVOF) thermally sprayed inconel-625 coatings on different metallic surfaces, *Surface and Coatings Technology* **200** (2006) 5782-5788. https://doi.org/10.1016/j.surfcoat.2005.08.143
[17] B. Wang, J. Gong, A. Y. Wang, C. Sun, R. F. Huang, L. S. Wen, Oxidation behaviour of NiCrAlY coatings on Ni-based superalloy, *Surface and Coatings Technology* **149** (2002) 70-75. https://doi.org/10.1016/S0257-8972(01)01427-X

[18] T. Aravind Nagaraj, S. P. K. Babu, M. Rajkumar, R. Mahendran, High temperature erosion behavior of cast nickel base 73Ni-13Cr-4Sn-4Bi-Mo alloy, *Materials Research Express* **6** (2019) . https://doi.org/10.1088/2053-1591/ab26d0

[19] Q. B. Nguyen, V. B. Nguyen, C. Y. H. Lim, Q. T. Trinh, S. Sankaranarayanan, Y. W. Zhang, M. Gupta, Effect of impact angle and testing time on erosion of stainless steel at higher velocities, *Wear* **321** (2014) 87-93. https://doi.org/10.1016/j.wear.2014.10.010

[20] G. T. Burstein, K. Sasaki, Effect of impact angle on the slurry erosion-corrosion of 304L stainless steel, *Wear* **240** (2000) 80-94. https://doi.org/10.1016/S0043-1648(00)00344-6

[21] C. P. Paul, S. K. Mishra, P. Tiwari, L. M. Kukreja, Solid-Particle Erosion Behaviour of WC/Ni Composite Clad layers with Different Contents of WC Particles, *Optics and Laser Technology* **50** (2013) 155-162. https://doi.org/10.1016/j.optlastec.2013.03.002

[22] M. Solecka, M. Kopyściański, J. Kusiński, A. Kopia, A. Radziszewska, Erosive wear of inconel 625 alloy coatings deposited by CMT method, *Archives of Metallurgy and Materials* **61** (2016) 1201-1206. https://doi.org/10.1515/amm-2016-0199

[23] N. Kamboj, L. Thakur, A study of the processing and characterization of RSM optimized YSZ-Inconel625 wear-resistant TIG weld cladding, *Surface Topography: Metrology and Properties* **10** (2022) 045021https://doi.org/10.1088/2051-672X/aca345

[24] H. Vasudev, L. Thakur, H. Singh, A. Bansal, Erosion behaviour of HVOF sprayed Alloy718-nano $Al_2O_3$ composite coatings on grey cast iron at elevated temperature conditions, *Surface Topography: Metrology and Properties* **9** (2021) 035022. https://doi.org/10.1088/2051-672X/ac1c80

[25] H. Vasudev, L. Thakur, H. Singh, A. Bansal, A study on processing and hot corrosion behaviour of HVOF sprayed Inconel718-nano $Al_2O_3$ coatings,*Materials Today Communications* **25** (2020) 101626. https://doi.org/10.1016/j.mtcomm.2020.101626

[26] G. Bi, C. N. Sun, M. L. Nai, J. Wei, Micro-structure and mechanical properties of nano-TiC reinforced Inconel 625 deposited using LAAM, *Physics Procedia* **41** (2013) 828-834. https://doi.org/10.1016/j.phpro.2013.03.155

[27] A. Keyvani, M. Saremi, M. H. Sohi, An investigation on oxidation, hot corrosion and mechanical properties of plasma-sprayed conventional and nanostructured YSZ coatings, *Surface and Coatings Technology* **206** (2011) 208-216. https://doi.org/10.1016/j.surfcoat.2011.06.036

[28] D. F. Zambrano, A. Barrios, L. E. Tobón, C. Serna, P. Gómez, J. D. Osorio, A. Toro, Thermal properties and phase stability of Yttria-Stabilized Zirconia (YSZ) coating deposited by Air Plasma Spray onto a Ni-base superalloy, *Ceramics International* **44** (2018) 3625-3635. https://doi.org/10.1016/j.ceramint.2017.11.109

[29] T. Dharini, P. Kuppusami, N. Kumar, D. D. Kumar, A. K. Soman, A. M. K. Kirubaharan, Tribological properties of YSZ and YSZ/Ni-YSZ nanocomposite coatings prepared by electron beam physical vapour deposition, *Ceramics International* **47** (2021) 26010-26018. https://doi.org/10.1016/j.ceramint.2021.06.006

[30] G. Prashar, H. Vasudev, Structure-property correlation and high-temperature erosion performance of Inconel625-$Al_2O_3$ plasma-sprayed bimodal composite coatings, *Surface and Coatings Technology* **439** (2022) 128450. https://doi.org/10.1016/j.surfcoat.2022.128450

[31] F. F. Lange, The interaction of a crack front with a second-phase dispersion, *Philosophical Magazine* **22** (1970) 983-992. https://doi.org/10.1080/14786437008221068

[32] F. F. Lange, Phase retention and fracture toughness of materials containing tetragonal $ZrO_2$, *Pergamon Press Ltd*, 1980. https://doi.org/10.1016/b978-1-4832-8414-9.50098-5